ACS Sustainable Chemistry & Engineering

Research Article

pubs.acs.org/journal/ascecg

Fluorination of Benzothiadiazole−Benzobisthiazole Copolymer Leads to Additive-Free Processing with Meliorated Solar Cell Performance

Anesh Gopal, Akinori Saeki,* Marina Ide, and Shu Seki*

†Department of Applied Chemistry, Graduate School of Engineering, Osaka University, 2-1 Yamadaoka, Suita, Osaka 565-0871, Japan

Supporting Information

ABSTRACT: Processing solvents and conditions have unique importance in the performance of bulk heterojunction organic solar cells. In the present work, we have investigated the role of a primary solvent and solvent additive in the device performance of two benzobisthiazole (BBTz)-based push−pull type polymers. In an inverted cell structure, the BBTz-*co*-fluorinated benzothiadiazole polymer (PBBTzFT) with a $PC_{71}BM$ acceptor showed additive-free enhanced performance with a power conversion efficiency (PCE) of 6.4% from a 1,2-dichlorobenzene solvent, while the BBTz-*co*-pyridylthiadiazole polymer (PBBTzPT) showed maximum performance from a chlorobenzene (CB) solution with a 1,8-diiodooctane (DIO) additive (PCE = 2.3%). The detailed investigation by atomic force microscopy and two-dimensional grazing incidence X-ray diffraction corroborates that the fluorination of benzothiadiazole brought about optimal morphology without a solvent additive, the PCE of which is comparable with the previous nonfluorinated analogue (PCE = 6.5%) processed from CB with DIO.

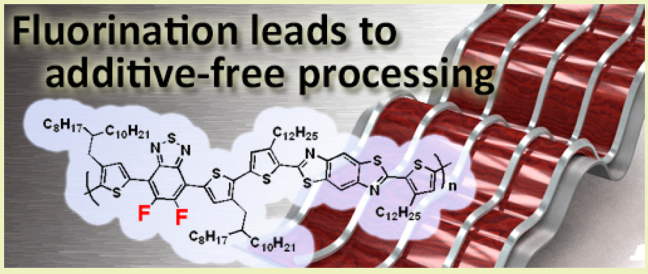

KEYWORDS: *Organic photovoltaic cell, 1,8-Diiodooctane (DIO), Time-resolved microwave conductivity (TRMC), Low bandgap polymer, X-ray diffraction*

INTRODUCTION

Organic photovoltaics (OPV) have substantial promise for giving clean and affordable energy sources in the future.[1,2] Enormous developments were perceived in this area during the past decade,[3−5] where the power conversion efficiency (PCE) of the polymer-based single bulk heterojunction (BHJ) devices significantly increased (∼9%),[6−9] and for the tandem cells, it has been approaching the benchmark for commercialization.[10−13] In general, the molecular design strategy includes tuning of the highest occupied molecular orbital (HOMO) of the donor polymer with that of the lowest unoccupied molecular orbital (LUMO) of the electron-accepting fullerene.[14−16] A deep-HOMO (−5.4 to −5.7 eV) polymer has an advantage of high open circuit voltage (V_{oc}).[17] Moreover, short circuit current density (J_{sc}) and fill factor (FF) are significantly influenced by BHJ morphology,[18,19] local polymer orientations at the donor/acceptor inteface,[20] and crystallinity and polymer orientation (face-on/edge-on) in the bulk,[21,22] which are generally controlled and optimized by solvent additives.[23−27]

From the practical roll-to-roll (R2R) process stand-point, single solvent processing is preferred over multi-solvent processing.[28] In addition, a thicker active layer is more relevant for the R2R process.[29,30] The recent studies show that polymer backbone modification with fluorine (F) substitution can improve PCE[31−33] due to (1) the strong dipole interaction between electropositive atom and electronegative F leading to strong polymer packing and preferential face-on orientations,[34] (2) the increased dipole of the electron-withdrawing unit of the copolymer assisting exciton dissociation,[35] and (3) fine-tuning of the energy alignment allowing marginal increase of V_{oc}.[36] Notably, fluorination sometimes offers a single additive-free solvent processing to achieve the optimized performance with a striking PCE of 6−9% .[37−41]

In this work, we have investigated the roles of the electron-withdrawing unit and solvent additives in the device performance of two new benzobisthiazole (BBTz)-based low band gap polymers. The BBTz polymers are known for their environmental stability, planarity, and electron-withdrawing nature,[42,43] which make it a promising conjugation unit in push−pull type semiconducting polymers.[44,45] In contrast, our previous study suggests that the BBTz moiety can act as a weak donor in combination with strong acceptor benzothiadiazole (BT),[46] demonstrating the PCE of 6.5% for the 1:2 blend film of PBBTzBT and [6,6]-phenyl C_{71} butyric acid methyl ester ($PC_{71}BM$) processed from chlorobenzene (CB) with a 3 v/v% solvent additive (1,8-diiodeoctane, DIO).[47] Inspired from that, we replaced BT either by pyridylthiadiazole (PT) or by fluorinated-benzothiadiazole (FT), affording PBBTzPT and PBBTzFT, respectively (Scheme 1). The device performances of these polymers were found to be significantly influenced by

Received: August 28, 2014
Revised: October 8, 2014
Published: October 9, 2014

   dx.doi.org/10.1021/sc5005617 | ACS Sustainable Chem. Eng. 2014, 2, 2613−2622

Scheme 1. Synthesis of PBBTzPT and PBBTzFT

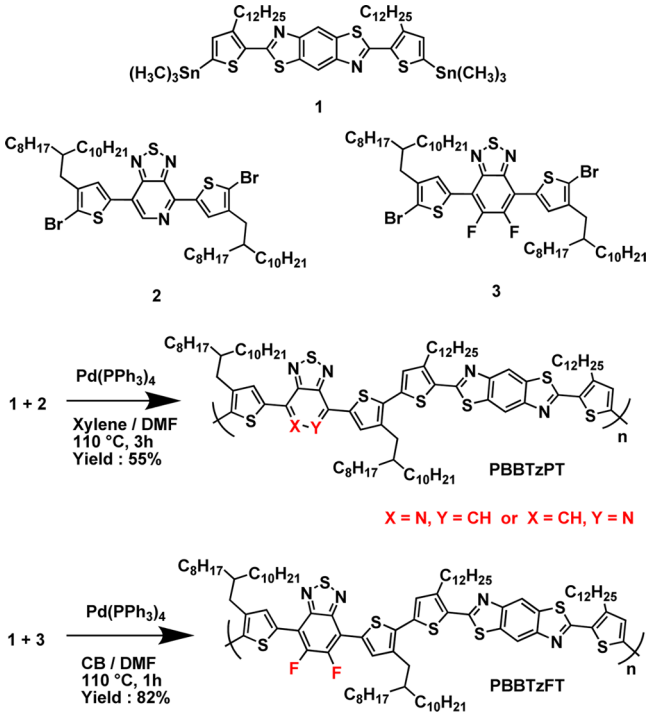

processing solvents. The PBBTzPT gave a maximum PCE in CB+DIO, while PBBTzFT showed additive-free enhancement in the 1,2-dichlorobenzene (DCB) solvent for a thick (200 nm) layer. Along with the noteworthy enhancement in V_{oc} compared with our previous PBBTzBT polymer, the differences in OPV output were discussed with the polymer orientation, BHJ morphology, and optoelectronic properties measured by Xe-flash time-resolved microwave conductivity (TRMC).[48]

EXPERIMENTAL SECTION

Materials and Instruments. Chemicals and solvents were purchased from Tokyo Chemical, Inc. (TCI) and Wako Chemical, Inc., respectively. Final purifications of the monomers were done by a recycle preparative HPLC system (Japan Analytical Industry Co., Ltd., LC-9210NEXT with JaiGel-1H/-2H) using $CHCl_3$ as eluent. The polymers were characterized by NMR spectroscopy (in chloroform-d) and gel permeation chromatography (GPC) using tetrahydrofuran (THF) eluent. NMR spectra were recorded on a JEOL 400SS (400 MHz) spectrometer, and all spectra were recorded in a $CDCl_3$ solution using TMS as the internal reference standard. All steady state absorption spectra were recorded on a Jasco V-570 UV−vis spectrophotometer. Photoelectron yield spectroscopy (PYS) experiments were done on a RIKEN Keiki Co., Ltd., model AC-3. AFM surface morphologies of the devices were obtained from a Seiko Instruments, Inc., model Nanocute OP, and Nanonavi II. 2D-GIXRD experiments were performed at the SPring-8 on beamline BL19B2 or BL46XU using a 12.39 keV (λ = 1 Å) X-ray. The 2D-GIXRD patterns of the devices were recorded with a 2D image detector (Pilatus 100 K). The percentage of face-on orientation was calculated using the equation face-on % = $(I_{ip}/(I_{op} + I_{ip})) \times 100$, where the I_{ip} and I_{op} are the signal intensities of (100) plane in the in-plane (q_{xy}) and out-of-plane (q_z) directions, respectively.[22]

Synthesis of Monomers and Polymers. The two polymers (PBBTzPT and PBBTzFT) were synthesized via Stille coupling as shown in Scheme 1. The monomers 2,6-bis(3-dodecyl-5-(trimethylstannyl)thiophen-2-yl)benzo[1,2-*d*:4,5-*d*′]bis(thiazole) (1),[45] 4,7-dibromo-[1,2,5]thiadiazolo[3,4-*c*]pyridine (2),[49] and 5,6-difluoro-4,7-diiodobenzo[c][1,2,5]thiadiazole (3)[50] were synthesized according to the previous reports.

Synthesis of PBBTzPT. In a 20 mL Schlenk flask, 2,6-bis(5-trimethyltin-3-dodecylthiophen-2-yl)-benzo[1,2-*d*;4,5-*d*′]bisthiazole (100 mg, 0.078 mmol) and 4,7-bis[5-bromo-4-(2-hexyldecyl)-2-thienyl]-2,1,3-benzothiadiazole (80 mg, 0.078 mmol) were dissolved in an anhydrous xylene (3 mL) and DMF (0.2 mL) solvent mixture. The reaction flask was degassed and refilled with nitrogen. $Pd(PPh_3)_4$ (1 mg, 1.23 μmol) was added to the flask under a nitrogen counter flow. The reaction mixture was refluxed at 110 °C for 4 h. Bromothiophene (0.05 mL) was added and continued refluxing for 1 h; then trimethylstannylthiophene (0.1 mL) was added and further refluxed for 1 h to complete the end-capping reaction. The resulting polymer solution was diluted by adding toluene (10 mL) and then being poured into anhydrous degassed methanol (100 mL) under stirring. The precipitate was filtered and dried in a vacuum oven. The polymer was dissolved in chlorobenzene and purified by column chromatography (the column alternatively packed with Celite, silica-NH and silica-NH_2) and then precipitated in methanol, filtered, and dried under vacuum. Soxhlet purification was performed in acetone and hexane for 6 h for each. Finally, the concentrated chlorobenzene solution was poured into acetone, and the precipitate was collected by filtration, affording a dark blue product (68 mg) with a yield of 55%. Weight-averaged molecular weight (M_w) = 65 kg mol^{-1}, number-averaged molecular weight (M_n) = 27 kg mol^{-1}, polydispersity index (PDI) = 2.3, ^{1}H NMR (400 MHz, 40 °C, $CDCl_3$) δ: 8.9−9.3 (br, 1H), 7.9−8.6 (br, 2H), 7.3−7.7 (br, 2H) 6.9−7.2 (br, 2H), 2.73−3.25 (br, 8H), 1.7−1.95 (br, 6H) 1.0−1.4 (br, 96H), 0.8−0.95 (br, 18H).

Synthesis of PBBTzFT. In a 20 mL Schlenk flask, 2,6-bis(5-trimethyltin-3-dodecylthiophen-2-yl)-benzo[1,2-*d*;4,5-*d*′]bisthiazole (50 mg, 0.049 mmol) and 4,7-bis(5-bromo-4-(2-octyldodecyl)-thiophen-2-yl)-5,6-difluorobenzo[c][1,2,5] thiadiazole (52 mg, 0.049 mmol) were dissolved in anhydrous chlorobenzene (1 mL) and DMF (0.2 mL) solvent mixture. The reaction flask was degassed and refilled with nitrogen. $Pd(PPh_3)_4$ (1 mg, 1.23 μmol) was added to the flask under a nitrogen counter flow. The reaction mixture was refluxed at 110 °C for 1 h. Bromothiophene (0.05 mL) was added and stirred continuously for another 1 h. Finally trimethylstannylthiophene (0.1 mL) was added and refluxed for 1 h to complete the end-capping reaction. The resulting polymer was purified by a series of precipitation and Soxhlet extraction as described for the previous polymer, affording a dark brown product (64 mg) with a 82% yield. GPC M_w = 237 kg mol^{-1}, M_n = 107 kg mol^{-1}, PDI = 2.2, ^{1}H NMR (400 MHz, 40 °C, $CDCl_3$) 7.9−8.4 (br, 4H), 6.8−7.1 (br, 2H), 2.72−3.21 (br, 8H), 1.8−2 (br, 6H) 1.0−1.4 (br, 96H), 0.8−0.9 (br, 18H).

Xe-Flash Time Resolved Microwave Conductivity Measurements. The experimental setup for the measurements can be found elsewhere.[48] The resonating frequency and power of the microwave were set at about 9.1 GHz and 3 mW, respectively, so that the electric field of the microwave was sufficiently small to not disturb the motion of charge carriers. White light pulse from a Xe flash lamp was used as the excitation source. The photoconductivity was calculated from the equation $\Delta\sigma = \Delta P_r/(AP_r)$, where ΔP_r, A, and P_r are the transient power change of reflected microwave from the resonant cavity, sensitivity factor, and reflected microwave power, respectively. The power of the white light pulse was 0.3 mJ cm^2 pulse^{-1}. The samples were prepared by drop-casting chlorobenzene (for PBBTzPT) or *o*-dichlorobenzene (for PBBTzFT) solutions of a polymer and $PC_{61}BM$ mixture at different weight ratios on a quartz plate. The samples were dried under vacuum. The Xe-TRMC experiments were performed under an ambient condition at room temperature.

Photovoltaic Device Fabrication and Measurements. The ITO-coated glass was first cleaned by ultrasonication with a series of solvents from diluted detergent, water, acetone, and isopropyl alcohol, dried under air stream, and UV/ozone-treated for 20 min. A ZnO layer was deposited on the ITO surface by using a reported sol−gel method[51] (0.1 g/mL zinc acetate dihydrate and 0.028 g/mL ethanolamine in 2-methoxyethanol). The ZnO solution was spin-coated and annealed at 200 °C for 30 min. A hot solution (80 °C) of a polymer and $PC_{61}BM$ or $PC_{71}BM$ (purchased from Frontier Carbon, Inc.) mixture was spin-coated on top of the ZnO layer from different solvents in a nitrogen atmosphere at 25 °C. The thickness of the active

layer was controlled by the rotation speed and measured by a surface profiler (ULVAC model Dektak 150). After spin-coating, the photoactive layer was transferred to an ultrahigh vacuum chamber and then waited at least for 30 min to remove residual solvent additive. On top of the active layer, 10 nm MoO_x and 100 nm Ag layers were sequentially deposited using a shadow mask by thermal evaporation. The final device configuration was an ITO (120−160 nm)/ZnO (30 nm)/BHJ active layer/MoO_x (10 nm)/Ag (100 nm) with an active area of 7.1 mm^2. Current−voltage (J−V) curves were measured using a source-measure unit (ADCMT Corp., 6241A) under AM 1.5 G solar illumination at 100 mW cm^{-2} (1 sun, monitored by a calibrated standard cell, Bunko Keiki SM-250 KD) from a 300 W solar simulator (SAN-EI Corp., XES-301S). The EQE spectra were measured by a Bunko Keiki model BS-520BK equipped with a Keithley model 2401 source meter. The monochromatic light power was calibrated by a silicon photovoltaic cell, Bunko Keiki model S1337−1010BQ.

RESULTS AND DISCUSSION

UV−Vis Absorption Studies. The UV−vis absorption spectra of PBBTzPT and PBBTzFT in solution and thin film are shown in Figure 1a, and the corresponding data obtained

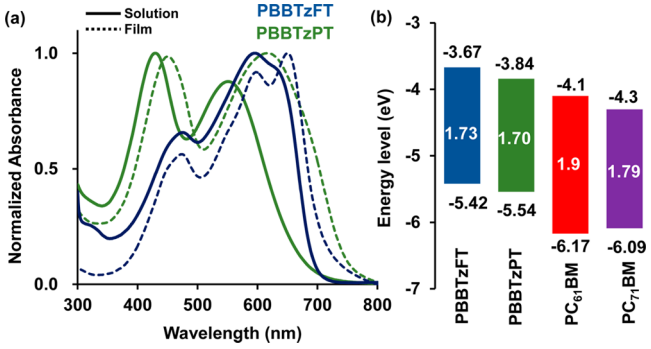

Figure 1. (a) UV−vis absorption spectra of PBBTzPT (green) and PBBTzFT (blue) in CB solution (solid lines) and thin film (dotted lines). (b) Energy diagram of the polymers and methanofullerenes.

are summarized in Table 1. PBBTzPT in the CB solution showed two absorption peaks at 426 and 548 nm, whereas in thin film, the peaks were red-shifted to 453 and 621 nm, respectively. The fluorinated derivative PBBTzFT in CB showed two absorption maxima at 474 and 594 nm. The longer absorption peak accompanied a shoulder band at 630 nm, which can be attributed to the intermolecular aggregation band.[51] In thin film, the aggregation band showed a 20 nm red shift with considerable enhancement in intensity, indicating its superiority in molecular ordering, which arises from the amplified interchain interactions induced by the fluorine atoms.[38] The optical band gaps (E_g^{opt}) of the polymers were calculated from the onset value of thin film UV−vis absorption spectrum and were found to be 1.70 and 1.73 eV for PBBTzPT and PBBTzFT, respectively (Figure 1b).

The HOMOs of the polymers were measured by photoelectron yield spectroscopy (PYS, Figure S1, Supporting Information). The PBBTzPT showed a slightly deeper HOMO level (−5.54 eV) in comparison with PBBTzFT (−5.42 eV). The strong electron accepting nature of the PT with that of the FT moiety[52] is responsible for the decreased HOMO level of PBBTzPT. The LUMO levels of the polymers were calculated from the HOMO energy levels and E_g^{opt}. The LUMO of the PBBTzPT was found to be −3.84 eV, and PBBTzFT showed a decreased LUMO level of −3.69 eV.

The density functional theory (DFT) calculations of PBBTzPT and PBBTzFT are depicted in Figure 2, which demonstrates nearly planar structures and well-distributed HOMO over conjugated backbone for both polymers. The electron density of the LUMO is localized on the electron deficient PT or FT moiety, validating that they are the electron-withdrawing units. The calculated HOMO and LUMO energy levels of the two polymers are in accordance with the experimental results.

Xe-Flash Time-Resolved Microwave Conductivity Experiments. The TRMC experiments can be effectively used to predict the photovoltaic performance of an organic semiconductor without fabricating a device.[53−56] A white light pulse from a Xe-flash lamp induces photoconductivity transient, the maximum of which ($\Delta\sigma_{max}$) includes the information about charge carrier lifetime, local charge carrier mobility, and charge carrier density.[48] By definition, $\Delta\sigma_{max} = e\Delta n_{max}(\mu_+ + \mu_-)$, where e is the elementary charge, Δn_{max} is the charge carrier density at photoconductivity maximum, and μ_+ and μ_- are hole mobility and electron mobility, respectively. In Xe-TRMC experiment shown in Figure 3a, the pristine PBBTzFT processed from DCB showed a 12 times enhanced photoconductivity ($\Delta\sigma_{max}$ = 1.6×10^{-9} S cm^{-1}) over PBBTzPT processed from CB ($\Delta\sigma_{max}$ = 1.2×10^{-10} S cm^{-1}), which clearly envisages the higher local charge carrier mobility of PBBTzFT than PBBTzPT. The HOMO/LUMO energy level diagram of the polymers (Figure 1b) suggests that both PBBTzPT and PBBTzFT can act as potential donors in combination with PCBM acceptors. Accordingly, the PBBTzPT showed a 65 fold increase in $\Delta\sigma_{max}$ when mixing with $PC_{61}BM$ at a 1:1 w/w% blend ratio (from 1.2×10^{-10} to 8.4×10^{-9} S cm^{-1}). The $\Delta\sigma_{max}$ value for PBBTzFT at a 1:1 blend ratio with $PC_{61}BM$ (3.3×10^{-8} S cm^{-1}) was also as high as 20-fold with respect to the pristine polymer. The higher $\Delta\sigma_{max}$ of the pristine and PCBM blend of PBBTzFT rather than PBBTzPT presumably resulted from the inherent charge transport along the polymer backbone and better BHJ network of the former. This might be partly associated with the higher molecular weight (M_w = 273 kg mol^{-1}) of PBBTzFT than that of PBBTzPT (65 kg mol^{-1}).

The superiority of PBBTzFT over PBBTzPT is clear from the $\Delta\sigma_{max}$ of each polymer at a 1:1 blend ratio, as shown in Figure 3b. In order to find the optimal blend ratio for maximum photovoltaic performance, we screened the blend ratio of the

Table 1. Absorption Maxima, Band Gap, and HOMO/LUMO Energies of PBBTzPT and PBBTzFT

	$\lambda_{max,abs}$(nm)				expt.[d] (calc.)[e] (eV)	
polymer	solution[a]	thin film[b]	onset[b] (nm)	E_g^{opt} (eV)[c]	HOMO	LUMO[f]
PBBTzPT	426, 548	453, 621	731	1.70	−5.54 (−4.92)	−3.84 (−3.13)
PBBTzFT	474, 594, 630	474, 603, 650	715	1.73	−5.42 (−4.94)	−3.69 (−2.99)

[a]Measured in CB. [b]Prepared on a quartz plate by spin-casting of CB polymer solution (1 wt %). [c]Determined by onset of optical absorption. [d]Measured by PYS. [e]DFT calculations by B3LYP/6-31G*. [f]Calculated by adding E_g^{opt} to HOMO.

dx.doi.org/10.1021/sc5005617 | ACS Sustainable Chem. Eng. 2014, 2, 2613−2622

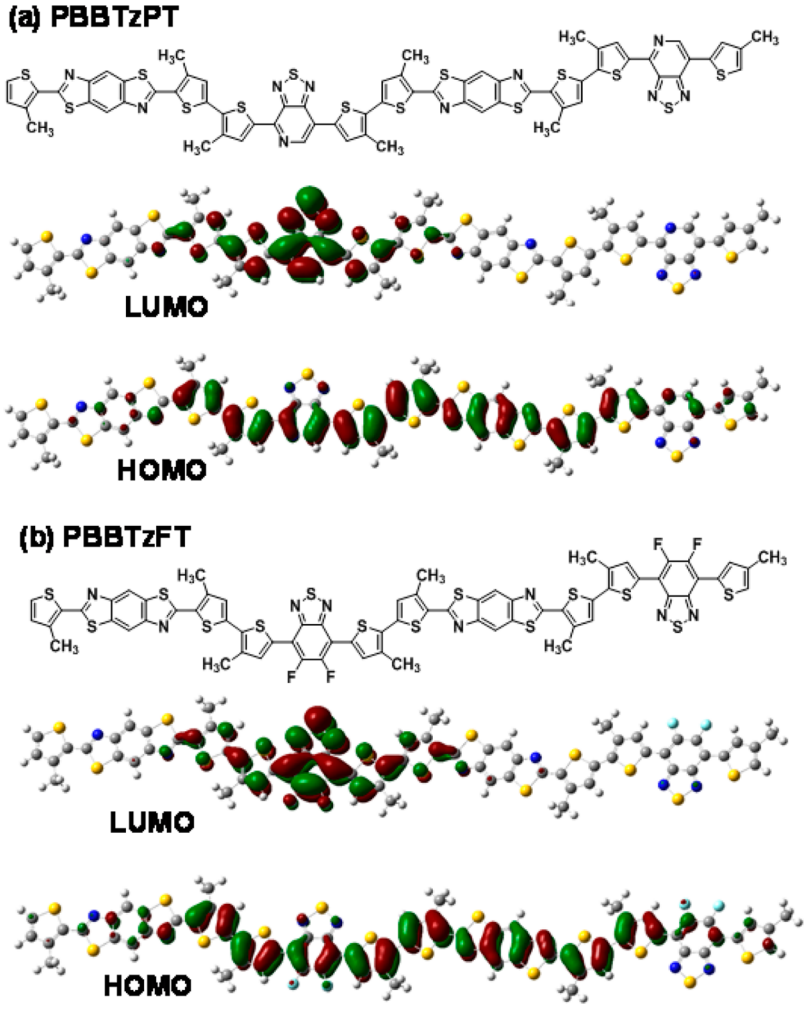

Figure 2. HOMO and LUMO of (a) PBBTzPT and (b) PBBTzFT obtained by DFT calculations using B3LYP/6-31G*. Side alkyl chains were replaced by methyl group for simplicity.

polymer and $PC_{61}BM$ (Figure 3b). The PBBTzFT showed an almost flat $\Delta\sigma_{max}$ over a wide range of $PC_{61}BM$ blend ratios (1:0.5−1:3), which proposes that the local charge carrier mobility of the polymers was insensitive to small variations in donor−acceptor (DA) blend ratios. Meanwhile, the PBBTzPT indicated two peaks at polymer-rich and PCBM-rich compositions (about 30 and 80 wt % PCBM, respectively), suggesting that hole and electron mobilities were impaired when the DA blend ratio gets closer to 1:1. The other processing conditions of CB+DIO and DCB were examined for PBBTzFT:$PC_{71}BM$ at a fixed DA ratio of 1:2 (Figure 3c). Interestingly, DCB indicated a higher $\Delta\sigma_{max}$ than that of CB +DIO. $PC_{71}BM$ instead of $PC_{61}BM$ generally leads to the better photoabsorption of visible light and increased J_{sc} of OPV device, thereby PBBTzFT:$PC_{71}BM$ processed from DCB is suggested to give the highest OPV performance. In contrast, the $\Delta\sigma_{max}$ of PBBTzFT was still much lower than that PBBTzFT even though it was processed from CB+DIO and blended with $PC_{71}BM$ (Figure 3d). Most importantly, we can predict that PBBTzFT should have much better OPV performance than PBBTzPT from the Xe-flash TRMC evaluation.

Photovoltaic Performances. The photovoltaic performance of PBBTzPT and PBBTzFT with $PC_{61(71)}BM$ acceptors were explored in different processing solvents, CB and DCB with/without DIO. By following the Xe-TRMC results, we have investigated the photovoltaic performance of the polymers at different DA blend ratios. Following the recent successful examples,[6,8,47] we have a selected inverted cell structure to evaluate the OPV performance. The device configuration is glass/ITO/ZnO/BHJ/MoO_x/Ag, and the details of fabrication are described in the Experimental Section. The OPV device performances were measured under AM1.5G illumination (100 mW cm^{-2}) and are summarized in Table 2. Initially, we have investigated the device performance of the polymers at a 1:2 blend ratio processed from a CB solution with 3 v/v% DIO. The PBBTzFT:$PC_{61}BM$ device showed a superior PCE of 4.92% along with a high V_{oc} of 0.92 V over the PBBTzPT:$PC_{61}BM$ device (PCE = 2.09%, V_{oc} = 0.81 V). Moreover, replacing $PC_{61}BM$ with a $PC_{71}BM$ acceptor leads to overall improvement in the device performance. The PBBTzPT:$PC_{71}BM$ device showed a PCE of 2.3%, and the PBBTzFT:$PC_{71}BM$ device showed a PCE of 6.14%. The marginal increase in PBBTzPT:$PC_{71}BM$ is coincident with the Xe-flash TRMC evaluation (Figure 3d). The increased photovoltaic performance of these devices, mainly the increase in J_{sc}, can be ascribed to the enhanced photo absorption of $PC_{71}BM$ over the $PC_{61}BM$ acceptor.[16] In CB without a solvent additive, PBBTzPT:$PC_{71}BM$ as well as PBBTzFT:$PC_{71}BM$

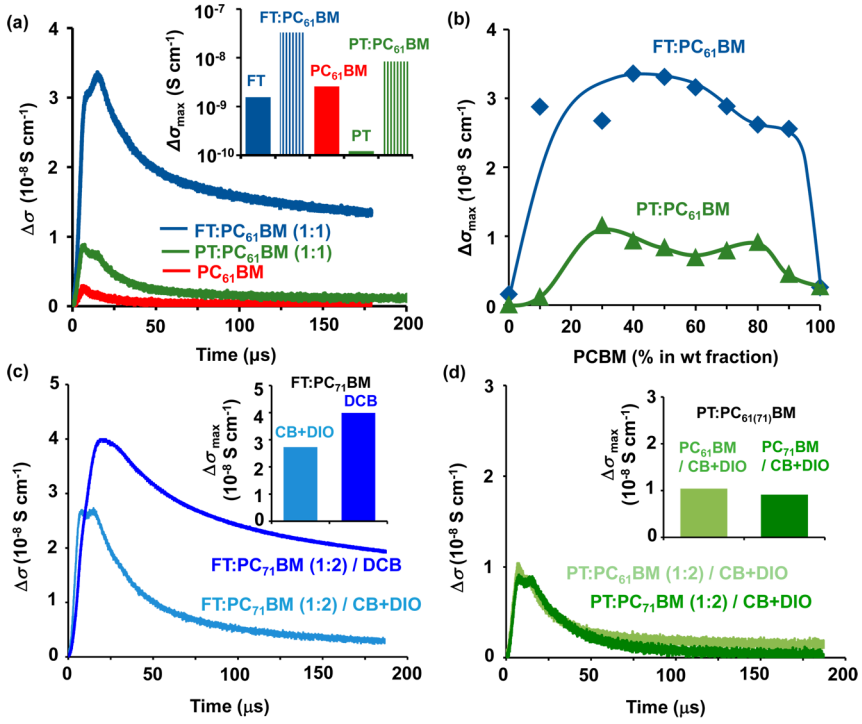

Figure 3. (a) Kinetic traces of transient photoconductivity ($\Delta\sigma$) for the blend of polymers (at a 1:1 ratio with $PC_{61}BM$) measured by Xe-TRMC. Inset shows the comparison of logarithmic $\Delta\sigma_{max}$ for PBBTzFT (abbreviated as FT processed from DCB) and PBBTzPT (abbreviated as PT processed from CB) with/without $PC_{61}BM$. (b) Plot of $\Delta\sigma_{max}$ versus wt % of $PC_{61}BM$. (c) $\Delta\sigma$ of PBBTzFT:$PC_{71}BM$ processed from CB+DIO (white blue) and DCB (blue). DIO concentration was 3 vol % otherwise noted. (d) $\Delta\sigma$ of PBBTzPT:$PC_{61}BM$ (white green) and PBBTzPT:$PC_{71}BM$ (green), both of which were processed from CB+DIO. All the thick TRMC films (>0.5 μm) were prepared by drop-casting.

Table 2. Summary of Photovoltaic Performance of PBBTzPT and PBBTzFT

polymer	acceptor	solvent[a]	blend ratio	L^b (nm)	J_{sc} (mA cm^{-2})	V_{oc} (V)	FF (%)	PCE[c] [PCE_{max}[d]] (%)
PBBTzPT	$PC_{61}BM$	CB+DIO	1:2	90 ± 10	4.35 ± 0.04	0.81 ± 0.01	54.0 ± 3.0	1.92 ± 0.14 (2.09)
	$PC_{71}BM$	CB+DIO	1:2	100 ± 10	5.91 ± 0.03	0.761 ± 0.021	48.0 ± 1.7	2.16 ± 0.13 (2.30)
	$PC_{71}BM$	CB	1:2	100 ± 10	1.18 ± 0.02	0.503 ± 0.01	36.0 ± 0.5	0.20 ± 0.01 (0.21)
	$PC_{71}BM$	DCB+DIO	1:2	105 ± 10	1.16 ± 0.01	0.305 ± 0.081	31.9 ± 2.5	0.15 ± 0.06 (0.42)
	$PC_{71}BM$	DCB	1:2	110 ± 10	1.28 ± 0.02	0.676 ± 0.067	41.3 ± 2.4	0.36 ± 0.06 (0.42)
	$PC_{71}BM$	CB+DIO	1:1.5	140 ± 20	4.52 ± 0.21	0.763 ± 0.004	46.9 ± 2.7	1.62 ± 0.16 (1.73)
PBBTzFT	$PC_{61}BM$	CB+DIO	1:2	200 ± 10	7.98 ± 0.04	0.919 ± 0.002	66.5 ± 0.4	4.88 ± 0.04 (4.92)
	$PC_{71}BM$	CB+DIO	1:2	210 ± 10	10.70 ± 0.12	0.885 ± 0.002	63.2 ± 0.9	5.99 ± 0.11 (6.14)
	$PC_{71}BM$	CB	1:2	200 ± 10	2.03 ± 0.04	0.900 ± 0.019	49.7 ± 1.4	0.87 ± 0.06 (0.94)
	$PC_{71}BM$	DCB+DIO	1:2	205 ± 10	9.95 ± 0.12	0.887 ± 0.002	58.6 ± 0.6	5.19 ± 0.12 (5.33)
	$PC_{71}BM$	DCB	1:2	210 ± 10	10.88 ± 0.45	0.881 ± 0.002	64.9 ± 1.2	6.21 ± 0.14 (6.37)
	$PC_{71}BM$	DCB	1:1.5	210 ± 10	8.64 ± 0.07	0.863 ± 0.005	58.8 ± 1.4	4.38 ± 0.06 (4.46)

[a]Films were prepared from CB or DCB with or without DIO (3 v/v%). [b]Photoactive layer thickness. [c]Based on minimum of four devices. [d]Maximum observed PCE.

showed below average PCE values of 0.21% and 0.85%, respectively.

Interestingly, when PBBTzFT was processed in a DCB solvent (PBBTzFT:$PC_{71}BM$(1:2)/DCB), the PCE of the device was further increased to 6.37%, owing to the slight increase in J_{sc} (10.88 mA cm^{-2}) and enhanced FF (64.9%), suggesting that DCB is a good processing solvent for PBBTzFT polymers. Of interest to note is that the device outputs of PBBTzFT:$PC_{71}BM$/CB+DIO and DCB are in line with the Xe-flash TRMC results (Figure 3c). The *JV* curves of the best performances under light and dark are displayed in Figure 4a and b, respectively. On the contrary, device performance of PBBTzPT in DCB (PBBTzPT:$PC_{71}BM$(1:2)/DCB) was diminished (PCE = 0.42%). From the above results, we were keen to know about the device performance of PBBTzFT in the DCB+DIO solvent mixture, and we found that PBBTzFT:$PC_{71}BM$(1:2)/DCB+DIO showed a decreased PCE of 5.33%. The significant decrease in PCE of the device was due to the decreased J_{sc} (9.95 mA cm^{-2}) and FF (58.6%), while the V_{oc} was not affected. When comparing the V_{oc}s of PBBTzFT and PBBTzPT at the best performing conditions (DCB and CB+DIO, respectively), PBBTzFT showed a 0.10 V higher value (0.88 V) than PBBTzPT (0.78 V), in spite of a 0.12 V deeper HOMO level of the latter (−5.54 eV for PBBTzPT and −5.42 eV for PBBTzFT). Because the difference in J_{sc} is only about half, the poor FF of PBBTzPT is responsible for the reduced V_{oc}. As dictated from the dark currents in Figure 4b, the reduced V_{oc} accompanied a large decrease in

dx.doi.org/10.1021/sc5005617 | ACS Sustainable Chem. Eng. 2014, 2, 2613−2622

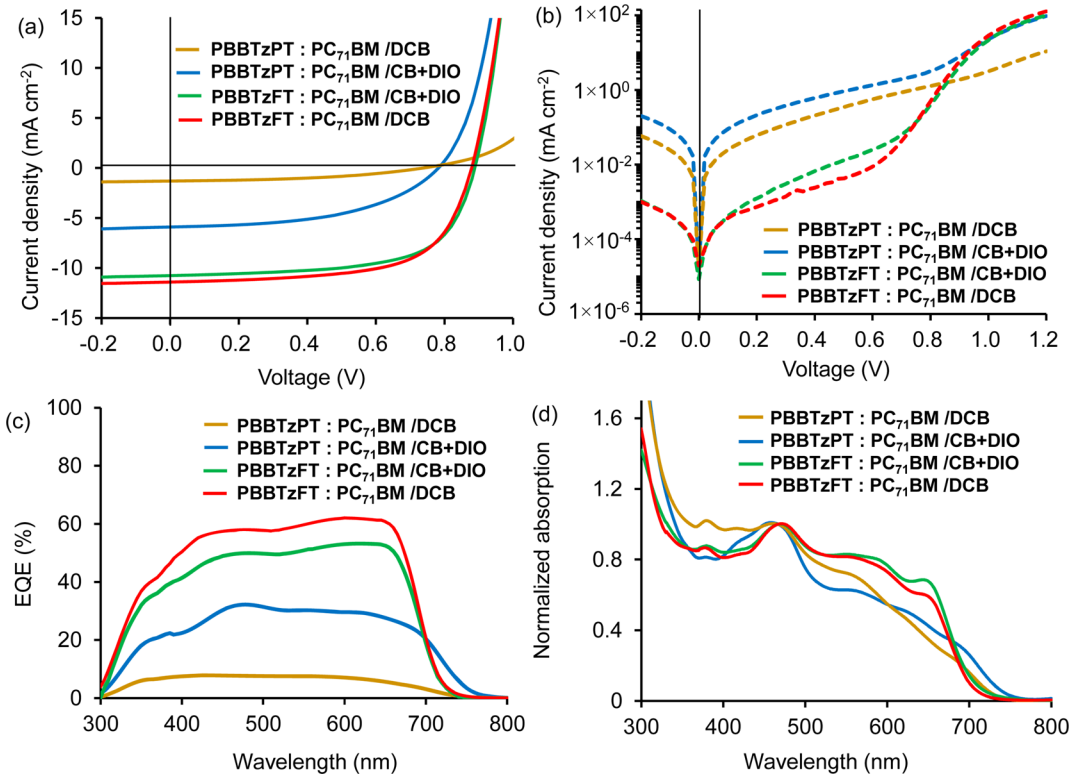

Figure 4. Photovoltaic performance of the polymers prepared from different processing solvents. (a) *J*–*V* characteristics of the devices under 1 sun illumination, (b) dark current density vs voltage of the devices, (c) EQE spectra, and (d) normalized (at 460 nm) UV–vis absorption spectrum of the devices.

parallel resistances (0.92 kΩ cm^{-2} for PBBTzPT and 345 kΩ cm^{-2} for PBBTzFT) and a small increase in series resistance (2.5 Ω cm^{-2} for PBBTzPT and 1.9 Ω cm^{-2} for PBBTzFT).

According to TRMC results, PBBTzFT is likely to preserve a high local charge carrier mobility even at lower fullerene content in the blend; therefore, we further explored the lower fullerene wt % (1:1.5 ratio) for the optimal solvent. The PBBTzPT:PC_{71}BM(1:1.5)/CB+DIO device showed a PCE of 1.62%, and PBBTzFT:PC_{71}BM(1:1.5)/DCB showed a PCE of 4.38%. The decrease in PCE suggests that the electron mobility of the active layer significantly contributed to the performance of the devices.

In order to understand the enhanced performance of the PBBTzFT:PC_{71}BM, we analyzed the external quantum efficiency (EQE) spectra (Figure 4c) and UV–vis absorption spectra (Figure 4d) of the devices. The normalized UV–vis absorption spectrum of the PBBTzFT:PC_{71}BM device showed a pronounced aggregation band at 655 nm for CB+DIO when compared with that processed from DCB. The EQE spectrum of these two devices showed identical characteristics with an almost flat region from 450 to 650 nm; however, the EQE spectrum of the DCB (maximum: 62%) is superior to the CB +DIO (maximum: 53%) over the whole wavelength. This envisions that the polymer BHJ morphology and/or polymer orientation are responsible for the improved OPV performance of the DCB-processed devices. On the other hand, PBBTzPT:PC_{71}BM revealed better device characteristics (*JV* curve under light and dark, EQE spectrum, and UV–vis absorption spectrum) in CB+DIO than in CB and DCB. This is a typical behavior of low bandgap polymers (LBP) when they are cast from solutions with a solvent additive.

Correlating the Polymer Orientation and Morphology with OPV Performance. The nanoscale morphology of the polymers in different processing solvents were probed by atomic force microscopic (AFM) analyses and are shown in Figure 5. The AFM images for the PBBTzPT:PC_{71}BM device showed about 400 nm-sized spherical structures with very high surface roughness of about 16 nm when processed in CB (Figure S2a, Supporting Information) and DCB (Figure S2b, Supporting Information), while those processed from CB+DIO showed a decreased surface roughness of about 3.9 nm with about 60 nm-sized particle-like features (Figures 5a and b). These are typical examples of unfavorable morphology, which impairs the exciton migration toward the polymer/fullerene interface and ultimately decreases the J_{sc} (<6 mA/cm^2). Divergently, the PBBTzFT:PC_{71}BM/CB+DIO device showed fiber-like structures with surface roughness of about 8.6 nm (Figure 5c). The phase image clearly visualizes the nanoscale fibers with 20–40 nm width (Figure 5d). Remarkably for the PBBTzFT:PC_{71}BM/DCB device, the nanofibers become more miscible with the reduced width of 10–20 nm and a surface roughness of about 4.4 nm (Figure 5e and f). In the case of the PBBTzFT:PC_{71}BM/DCB+DIO device, the size of the nanofibers and the surface roughness were slightly increased in comparison with those without DIO, which is consistent with the decrease in PCE (Figure S3, Supporting Information).

Adding a solvent additive is effective process engineering for LBP by driving the excessive phase separation or homogeneous mixing toward the desired BHJ having a hierarchical and percolated nanoscale network.[19] In contrast, crystalline poly(3-hexylthiophene) and a small number of LBP do not require a solvent additive because they can push the PCBM away from the crystalline polymer domains, which works as a driving force

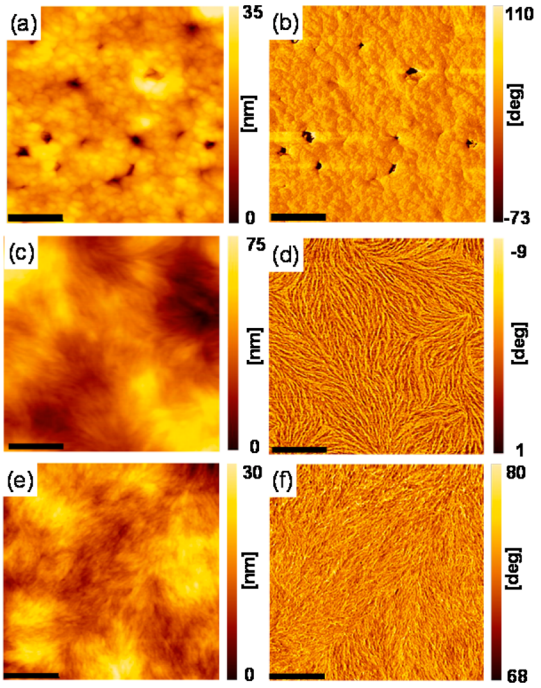

Figure 5. AFM height (left panel) and phase (right panel) images of (a, b) PBBTzPT:$PC_{71}BM$(1:2)/CB+DIO, (c, d) PBBTzFT:$PC_{71}BM$-(1:2)/CB+DIO solvent mixture, and (e,f) PBBTzFT:$PC_{71}BM$(1:2)/DCB. Scale bars are 500 nm in length.

for forming optimal BHJ morphology.[57,58] The solvent additive effect observed in PBBTzPT is similar to those of numerous LBPs, while the additive-free performance of PBBTzFT is in accordance with the crystalline polymers rather than the semicrystalline or amorphous LBPs. From the above observations, it is assumed that the remaining DIO after spin-coating reduces the solubility of the high molecular weight PBBTzFT polymer and that may lead to excessive intermolecular stacking and increases in the size of the nanoscale fibers.

To correlate the device performance with polymer orientation in the active layer, we performed two-dimensional grazing-incidence X-ray diffraction analysis (2D-GIXRD), shown in Figure 6. The percentages of polymer face-on orientations were roughly estimated from the signal intensities of 100 planes (interlamellar diffraction), out-of-plane (q_z axis) and in-plane (q_{xy} axis) (see Experimental Section).[22,59] The pristine PBBTzPT polymer showed a semicrystalline diffraction pattern corresponding to a 43% face-on orientation with a π-stacking distance of 3.8 Å and interlamellar distance of 23.7 Å (Figure 6a). The pristine PBBTzFT film showed an equivalent face-on orientation of 44%, while its diffraction is more intense and sharp than that of PBBTzPT. The full-width at the half-maxima (fwhm) of in-plane (100) diffractions were 2θ = 0.34 and 0.96° for PBBTzFT and PBBTzPT, respectively, suggesting a higher crystallinity for PBBTzFT than PBBTzPT, consistent with the AFM observation (Figure 5). In addition, the π-stacking distance of PBBTzFT was found to be as small as 3.6 Å with an interlamellar distance of 24.8 Å (Figure 6c). The active layer of the PBBTzPT:$PC_{71}BM$(1:2)/CB+DIO device showed a broad and weak diffraction pattern, indicative of its amorphous nature. The best performing PBBTzFT:$PC_{71}BM$-(1:2)/DCB device showed a decreased face-on orientation of 21% with preserved π-stacking distance of 3.6 Å and an interlamellar distance of 25.4 Å (Figure 6d), which indicates that upon mixing with fullerene the percentage of face-on orientation of PBBTzFT was significantly reduced. On the other hand, the PBBTzFT:$PC_{71}BM$(1:2) with solvent additives (DCB+DIO and CB+DIO) showed face-on orientations of 48% and 53%, respectively (Figure S4, Supporting Information). From these results, we can conclude that the additive-free maximized PCE for PBBTzFT:$PC_{71}BM$ in DCB is due to the optimized BHJ network with more miscible and smaller polymer nanofibers, which contributes to the increased J_{sc} and FF. Both preferable face-on orientation and miscible polymer nanofibers are essential for further improvement of OPV device; however, in the present case, they were found unable to be simultaneously achieved by the two processing conditions (DCB or CB+DIO). The use of DIO can preserve the face-on orientation, while the BHJ network was degraded. On the contrary, pure DCB leads to better BHJ morphology, while it reduced the percentage of face-on orientation.

CONCLUSIONS

Two new benzobisthiazole (BBTz)-based LBPs were synthesized with different acceptor strength units (PBBTzPT and PBBTzFT), both of which have concurrently deep HOMOs

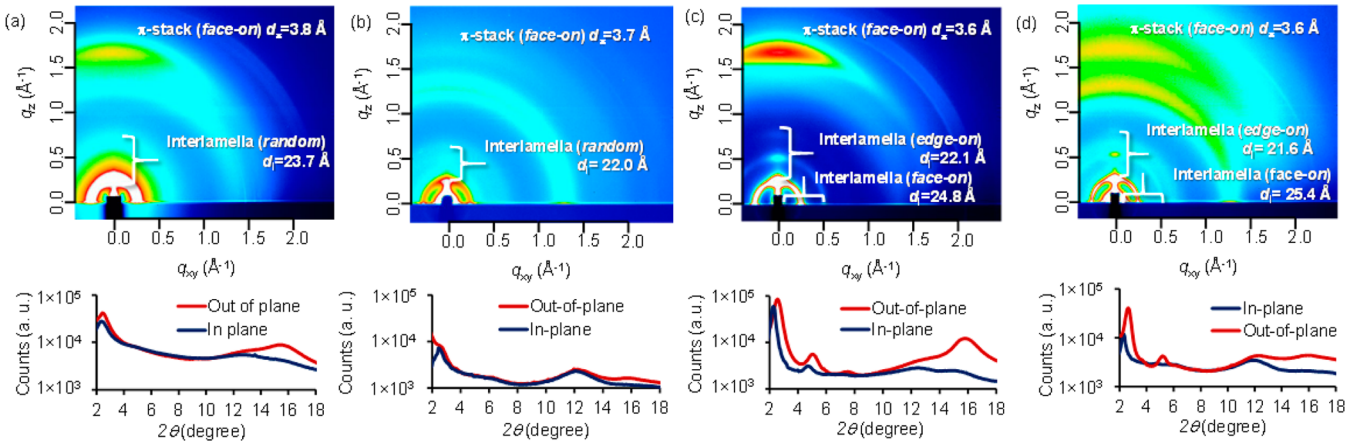

Figure 6. 2D-GIXRD of pristine and BHJ films for PBBTzPT and PBBTzFT polymers. (a) PBBTzPT/CB, (b) PBBTzPT:$PC_{71}BM$(1:2)/CB+DIO, (c) PBBTzFT/DCB, and (d) PBBTzFT:$PC_{71}BM$(1:2)/DCB. Corresponding out-of-plane (red) and in-plane (dark blue) GIXRD patterns are shown in the lower panel.

dx.doi.org/10.1021/sc5005617 | ACS Sustainable Chem. Eng. 2014, 2, 2613−2622

(−5.5 and −5.4 eV) and low bandgap energies (1.70 and 1.73 eV). On the basis of the guide provided by the deviceless evaluation of Xe-TRMC, we examined the device performance of these polymers with different processing solvents. It was found that the PCEs of the PBBTzPT:$PC_{71}BM$ devices constrained around 2% even in the presence of the DIO additive. In contrast, the PBBTzFT:$PC_{71}BM$(1:2) showed a notable jump in PCE to 6.37% (average: 6.21%) when prepared from an additive-free DCB solution. Processing from a CB +DIO solution also demonstrated a comparable PCE of 6.14% (average: 5.99%). The AFM morphological analysis revealed that the DCB-processed active layer showed an enhanced nanoscale morphology compared with the CB+DIO processed one, although 2D-GIXRD results identified that the DCB processed cell has a less face-on orientation percentage than the CB+DIO processed cell. Therefore, the fluorination of benzobisthiazole offers additive-free processing with meliorated solar cell performance, which is more compatible with the cost-effective R2R fabrication than additive-mediated film processing.

■ ASSOCIATED CONTENT

Ⓢ Supporting Information

Additional data of PYS spectra, AFM images, and 2D-GIXRD images. This material is available free of charge via the Internet at http://pubs.acs.org.

■ AUTHOR INFORMATION

Corresponding Authors

*E-mail: saeki@chem.eng.osaka-u.ac.jp (A.S.).
*E-mail: seki@chem.eng.osaka-u.ac.jp (S.S.).

Notes

The authors declare no competing financial interest.

■ ACKNOWLEDGMENTS

This work was supported by a KAKENHI grant from the Ministry of Education, Culture, Sports, Science and Technology (MEXT) of Japan, and a research grant from Toyota Physical & Chemical Research Institute Scholars, Japan. The authors thank Dr. Tomoyuki Koganezawa at Japan Synchrotron Radiation Research Institute, Japan, and Dr. Itaru Osaka at RIKEN, Japan, for the 2D-GIXRD experiments (Proposals 2013B1719 and 2014A1530).

■ REFERENCES

(1) Graetzel, M.; Janssen, R. A.; Mitzi, D. B.; Sargent, E. H. Materials interface engineering for solution-processed photovoltaics. *Nature* **2012**, *488*, 304−312.

(2) Li, G.; Zhu, R.; Yang, Y. Polymer solar cells. *Nat. Photonics* **2012**, *6*, 153−161.

(3) Cheng, Y. J.; Yang, S. H.; Hsu, C. S. Synthesis of conjugated polymers for organic solar cell applications. *Chem. Rev.* **2009**, *109*, 5868−5923.

(4) Boudreault, P.-L. T.; Najari, A.; Leclerc, M. Processable low-bandgap polymers for photovoltaic applications. *Chem. Mater.* **2011**, *23*, 456−469.

(5) Dou, L.; You, J.; Hong, Z.; Xu, Z.; Li, G.; Street, R. A.; Yang, Y. 25th anniversary article: A decade of organic/polymeric photovoltaic research. *Adv. Mater.* **2013**, *25*, 6642−6671.

(6) He, Z.; Zhong, C.; Su, S.; Xu, M.; Wu, H.; Cao, Y. Enhanced power-conversion efficiency in polymer solar cells using an inverted device structure. *Nat. Photonics* **2012**, *6*, 593−597.

(7) Zhang, M.; Gu, Y.; Guo, X.; Liu, F.; Zhang, S.; Huo, L.; Russell, T. P.; Hou, J. Efficient polymer solar cells based on benzothiadiazole and alkylphenyl substituted benzodithiophene with a power conversion efficiency over 8%. *Adv. Mater.* **2013**, *25*, 4944−4949.

(8) Woo, S.; Kim, W. H.; Kim, H.; Yi, Y.; Lyu, H. K.; Kim, Y. 8.9% Single-stack inverted polymer solar cells with electron-rich polymer nanolayer-modified inorganic electron-collecting buffer layers. *Adv. Energy Mater.* **2014**, *4*, 1301692.

(9) Chao, Y. H.; Jheng, J. F.; Wu, J. S.; Wu, K. Y.; Peng, H. H.; Tsai, M. C.; Wang, C. L.; Hsiao, Y. N.; Wang, C. L.; Lin, C. Y.; Hsu, C. S. Porphyrin-incorporated 2D D-A polymers with over 8.5% polymer solar cell efficiency. *Adv. Mater.* **2014**, *26*, 5205−5210.

(10) You, J.; Chen, C. C.; Hong, Z.; Yoshimura, K.; Ohya, K.; Xu, R.; Ye, S.; Gao, J.; Li, G.; Yang, Y. 10.2% power conversion efficiency polymer tandem solar cells consisting of two identical sub-cells. *Adv. Mater.* **2013**, *25*, 3973−3978.

(11) Li, K.; Li, Z.; Feng, K.; Xu, X.; Wang, L.; Peng, Q. Development of large band-gap conjugated copolymers for efficient regular single and tandem organic solar cells. *J. Am. Chem. Soc.* **2013**, *135*, 13549−13557.

(12) Li, W.; Furlan, A.; Hendriks, K. H.; Wienk, M. M.; Janssen, R. A. Efficient tandem and triple-junction polymer solar cells. *J. Am. Chem. Soc.* **2013**, *135*, 5529−5532.

(13) You, J.; Dou, L.; Yoshimura, K.; Kato, T.; Ohya, K.; Moriarty, T.; Emery, K.; Chen, C. C.; Gao, J.; Li, G.; Yang, Y. A polymer tandem solar cell with 10.6% power conversion efficiency. *Nat. Commun.* **2013**, *4*, 1446−1456.

(14) Mei, J.; Bao, Z. Side chain engineering in solution-processable conjugated polymers. *Chem. Mater.* **2014**, *26*, 604−615.

(15) Scharber, M. C.; Mühlbacher, D.; Koppe, M.; Denk, P.; Waldauf, C.; Heeger, A. J.; Brabec, C. J. Design rules for donors in bulk-heterojunction solar cells—Towards 10% energy-conversion efficiency. *Adv. Mater.* **2006**, *18*, 789−794.

(16) Thompson, B. C.; Frechet, J. M. Polymer−fullerene composite solar cells. *Angew. Chem., Int. Ed.* **2008**, *47*, 58−77.

(17) Jo, J.; Pron, A.; Berrouard, P.; Leong, W. L.; Yuen, J. D.; Moon, J. S.; Leclerc, M.; Heeger, A. J. A new terthiophene−thienopyrrolodione copolymer-based bulk heterojunction solar cell with high open-circuit voltage. *Adv. Energy Mater.* **2012**, *2*, 1397−1403.

(18) Chen, L.-M.; Hong, Z.; Li, G.; Yang, Y. Recent progress in polymer solar cells: Manipulation of polymer:fullerene morphology and the formation of efficient inverted polymer solar cells. *Adv. Mater.* **2009**, *21*, 1434−1449.

(19) Huang, Y.; Kramer, E. J.; Heeger, A. J.; Bazan, G. C. Bulk heterojunction solar cells: Morphology and performance relationships. *Chem. Rev.* **2014**, *114*, 7006−7043.

(20) Tumbleston, J. R.; Collins, B. A.; Yang, L. Q.; Stuart, A. C.; Gann, E.; Ma, W.; You, W.; Ade, H. The influence of molecular orientation on organic bulk heterojunction solar cells. *Nat. Photonics* **2014**, *8*, 385−391.

(21) Ma, W.; Tumbleston, J. R.; Wang, M.; Gann, E.; Huang, F.; Ade, H. Domain purity, miscibility, and molecular orientation at donor/acceptor interfaces in high performance organic solar cells: paths to further improvement. *Adv. Energy Mater.* **2013**, *3*, 864−872.

(22) Osaka, I.; Saito, M.; Koganezawa, T.; Takimiya, K. Thiophene-thiazolothiazole copolymers: Significant impact of side chain composition on backbone orientation and solar cell performances. *Adv. Mater.* **2014**, *26*, 331−338.

(23) Lee, J. K.; Ma, W. L.; Brabec, C. J.; Yuen, J.; Moon, J. S.; Kim, J. Y.; Lee, K.; Bazan, G. C.; Heeger, A. J. Processing additives for improved efficiency from bulk heterojunction solar cells. *J. Am. Chem. Soc.* **2008**, *130*, 3619−3623.

(24) Rogers, J. T.; Schmidt, K.; Toney, M. F.; Kramer, E. J.; Bazan, G. C. Structural order in bulk heterojunction films prepared with solvent additives. *Adv. Mater.* **2011**, *23*, 2284−2288.

(25) Guo, X.; Cui, C.; Zhang, M.; Huo, L.; Huang, Y.; Hou, J.; Li, Y. High efficiency polymer solar cells based on poly(3-hexylthiophene)/indene-C70 bisadduct with solvent additive. *Energy Environ. Sci.* **2012**, *5*, 7943−7949.

(26) Graham, K. R.; Wieruszewski, P. M.; Stalder, R.; Hartel, M. J.; Mei, J.; So, F.; Reynolds, J. R. Improved performance of molecular

bulk-heterojunction photovoltaic cells through predictable selection of solvent additives. *Adv. Funct. Mater.* **2012**, *22*, 4801−4813.
(27) Schmidt, K.; Tassone, C. J.; Niskala, J. R.; Yiu, A. T.; Lee, O. P.; Weiss, T. M.; Wang, C.; Frechet, J. M.; Beaujuge, P. M.; Toney, M. F. A mechanistic understanding of processing additive-induced efficiency enhancement in bulk heterojunction organic solar cells. *Adv. Mater.* **2014**, *26*, 300−305.
(28) Po, R.; Bernardi, A.; Calabrese, A.; Carbonera, C.; Corso, G.; Pellegrino, A. From lab to fab: How must the polymer solar cell materials design change? An industrial perspective. *Energy Environ. Sci.* **2014**, *7*, 925−943.
(29) Peet, J.; Wen, L.; Byrne, P.; Rodman, S.; Forberich, K.; Shao, Y.; Drolet, N.; Gaudiana, R.; Dennler, G.; Waller, D. Bulk heterojunction solar cells with thick active layers and high fill factors enabled by a bithiophene-co-thiazolothiazole push-pull copolymer. *Appl. Phys. Lett.* **2011**, *98*, 043301/1−3.
(30) Søndergaard, R.; Hösel, M.; Angmo, D.; Larsen-Olsen, T. T.; Krebs, F. C. Roll-to-roll fabrication of polymer solar cells. *Mater. Today* **2012**, *15*, 36−49.
(31) Chen, H.-C.; Chen, Y.-H.; Liu, C.-C.; Chien, Y.-C.; Chou, S.-W.; Chou, P.-T. Prominent short-circuit currents of fluorinated quinoxaline-based copolymer solar cells with a power conversion efficiency of 8.0%. *Chem. Mater.* **2012**, *24*, 4766−4772.
(32) Albrecht, S.; Janietz, S.; Schindler, W.; Frisch, J.; Kurpiers, J.; Kniepert, J.; Inal, S.; Pingel, P.; Fostiropoulos, K.; Koch, N.; Neher, D. Fluorinated copolymer PCPDTBT with enhanced open-circuit voltage and reduced recombination for highly eficient polymer solar cells. *J. Am. Chem. Soc.* **2012**, *134*, 14932−14944.
(33) Qin, T.; Zajaczkowski, W.; Pisula, W.; Baumgarten, M.; Chen, M.; Gao, M.; Wilson, G.; Easton, C. D.; Mullen, K.; Watkins, S. E. Tailored donor-acceptor polymers with an A-D1-A-D2 structure: controlling intermolecular interactions to enable enhanced polymer photovoltaic devices. *J. Am. Chem. Soc.* **2014**, *136*, 6049−6055.
(34) Stuart, A. C.; Tumbleston, J. R.; Zhou, H.; Li, W.; Liu, S.; Ade, H.; You, W. Fluorine substituents reduce charge recombination and drive structure and morphology development in polymer solar cells. *J. Am. Chem. Soc.* **2013**, *135*, 1806−1815.
(35) Rolczynski, B. S.; Szarko, J. M.; Son, H. J.; Liang, Y.; Yu, L.; Chen, L. X. Ultrafast intramolecular exciton splitting dynamics in isolated low-band-gap polymers and their implications in photovoltaic materials design. *J. Am. Chem. Soc.* **2012**, *134*, 4142−4152.
(36) Chen, H. Y.; Hou, J. H.; Zhang, S. Q.; Liang, Y. Y.; Yang, G. W.; Yang, Y.; Yu, L. P.; Wu, Y.; Li, G. Polymer solar cells with enhanced open-circuit voltage and efficiency. *Nat. Photonics* **2009**, *3*, 649−653.
(37) Zhou, H.; Yang, L.; Stuart, A. C.; Price, S. C.; Liu, S.; You, W. Development of fluorinated benzothiadiazole as a structural unit for a polymer solar cell of 7% efficiency. *Angew. Chem., Int. Ed.* **2011**, *50*, 2995−2998.
(38) Price, S. C.; Stuart, A. C.; Yang, L.; Zhou, H.; You, W. Fluorine substituted conjugated polymer of medium band gap yields 7% efficiency in polymer-fullerene solar cells. *J. Am. Chem. Soc.* **2011**, *133*, 4625−4631.
(39) Wang, N.; Chen, Z.; Wei, W.; Jiang, Z. Fluorinated benzothiadiazole-based conjugated polymers for high-performance polymer solar cells without any processing additives or post-treatments. *J. Am. Chem. Soc.* **2013**, *135*, 17060−17068.
(40) Tumbleston, J. R.; Stuart, A. C.; Gann, E.; You, W.; Ade, H. Fluorinated polymer yields high organic solar cell performance for a wide range of morphologies. *Adv. Funct. Mater.* **2013**, *23*, 3463−3470.
(41) Nguyen, T. L.; Choi, H.; Ko, S. J.; Uddin, M. A.; Walker, B.; Yum, S.; Jeong, J. E.; Yun, M. H.; Shin, T. J.; Hwang, S.; Kim, J. Y.; Woo, H. Y. Semi-crystalline photovoltaic polymers with efficiency exceeding 9% in a similar to 300 nm thick conventional single-cell device. *Energy Environ. Sci.* **2014**, *7*, 3040−3051.
(42) Osaheni, J. A.; Jenekhe, S. A. Electroactive and photoactive rod-coil copolymers - design, synthesis, and supramolecular regulation of photophysical properties. *J. Am. Chem. Soc.* **1995**, *117*, 7389−7398.
(43) Babel, A.; Jenekhe, S. A. High electron mobility in ladder polymer field-effect transistors. *J. Am. Chem. Soc.* **2003**, *125*, 13656−13657.
(44) Osaka, I.; Takimiya, K.; McCullough, R. D. Benzobisthiazole-based semiconducting copolymers showing excellent environmental stability in high-humidity air. *Adv. Mater.* **2010**, *22*, 4993−4997.
(45) Ahmed, E.; Subramaniyan, S.; Kim, F. S.; Xin, H.; Jenekhe, S. A. Benzobisthiazole-based donor−acceptor copolymer semiconductors for photovoltaic cells and highly stable field-effect transistors. *Macromolecules* **2011**, *44*, 7207−7219.
(46) Tsuji, M.; Saeki, A.; Koizumi, Y.; Matsuyama, N.; Vijayakumar, C.; Seki, S. Benzobisthiazole as weak donor for improved photovoltaic performance: microwave conductivity technique assisted molecular engineering. *Adv. Funct. Mater.* **2014**, *24*, 28−36.
(47) Saeki, A.; Tsuji, M.; Yoshikawa, S.; Gopal, A.; Seki, S. Boosting photovoltaic performance of a benzobisthiazole based copolymer: a device approach using a zinc oxide electron transport layer. *J. Mater. Chem. A* **2014**, *2*, 6075−6080.
(48) Saeki, A.; Yoshikawa, S.; Tsuji, M.; Koizumi, Y.; Ide, M.; Vijayakumar, C.; Seki, S. A versatile approach to organic photovoltaics evaluation using white light pulse and microwave conductivity. *J. Am. Chem. Soc.* **2012**, *134*, 19035−19042.
(49) Blouin, N.; Michaud, A.; Gendron, D.; Wakim, S.; Blair, E.; Neagu-Plesu, R.; Belletete, M.; Durocher, G.; Tao, Y.; Leclerc, M. Toward a rational design of poly(2,7-carbazole) derivatives for solar cells. *J. Am. Chem. Soc.* **2008**, *130*, 732−742.
(50) Wang, Y.; Xin, X.; Lu, Y.; Xiao, T.; Xu, X.; Zhao, N.; Hu, X.; Ong, B. S.; Ng, S. C. Substituent effects on physical and photovoltaic properties of 5,6-difluorobenzo[c][1,2,5]thiadiazole-based D-A polymers: Toward a donor design for high performance polymer solar cells. *Macromolecules* **2013**, *46*, 9587−9592.
(51) Park, H.-Y.; Lim, D.; Kim, K.-D.; Jang, S.-Y. Performance optimization of low-temperature-annealed solution-processable ZnO buffer layers for inverted polymer solar cells. *J. Mater. Chem. A* **2013**, *1*, 6327−6334.
(52) Yau, C. P.; Fei, Z.; Ashraf, R. S.; Shahid, M.; Watkins, S. E.; Pattanasattayavong, P.; Anthopoulos, T. D.; Gregoriou, V. G.; Chochos, C. L.; Heeney, M. Influence of the electron deficient co-monomer on the optoelectronic properties and photovoltaic performance of dithienogermole-based co-polymers. *Adv. Funct. Mater.* **2014**, *24*, 678−687.
(53) Grozema, F. C.; Siebbeles, L. D. A. Charge mobilities in conjugated polymers measured by pulse radiolysis time-resolved microwave conductivity: From single chains to solids. *J. Phys. Chem. Lett.* **2011**, *2*, 2951−2958.
(54) Rance, W. L.; Ferguson, A. J.; McCarthy-Ward, T.; Heeney, M.; Ginley, D. S.; Olson, D. C. Rumbles, G.; Kopidakis, N. Photoinduced carrier generation and decay dynamics in intercalated and non-intercalated polymer:fullerene bulk heterojunctions. *ACS Nano* **2011**, *5*, 5635−5646.
(55) Saeki, A.; Tsuji, M.; Seki, S. Direct evaluation of intrinsic optoelectronic performance of organic photovoltaic cells with minimizing impurity and degradation effects. *Adv. Energy Mater.* **2011**, *1*, 661−669.
(56) Aguirre, J. C.; Arntsen, C.; Hernandez, S.; Huber, R.; Nardes, A. M.; Halim, M.; Kilbride, D.; Rubin, Y.; Tolbert, S. H.; Kopidakis, N.; Schwartz, B. J.; Neuhauser, D. Understanding local and macroscopic electron mobilities in the fullerene network of conjugated polymer-based solar cells: Time-resolved microwave conductivity and theory. *Adv. Funct. Mater.* **2014**, *24*, 784−792.
(57) Treat, N. D.; Brady, M. A.; Smith, G.; Toney, M. F.; Kramer, E. J.; Hawker, C. J.; Chabinyc, M. L. Interdiffusion of PCBM and P3HT reveals miscibility in a photovoltaically active blend. *Adv. Energy Mater.* **2011**, *1*, 82−89.
(58) Jo, J.; Kim, S.-S.; Na, S.-I.; Yu, B.-K.; Kim, D.-Y. Time-dependent morphology evolution by annealing processes on polymer:-fullerene blend solar cells. *Adv. Funct. Mater.* **2009**, *19*, 866−874.
(59) Rivnay, J.; Mannsfeld, S. C.; Miller, C. E.; Salleo, A.; Toney, M. F. Quantitative determination of organic semiconductor micro-

structure from the molecular to device scale. *Chem. Rev.* **2012**, *112*, 5488−5519.